Electrochemically synthesized silver phosphate coating on anodized aluminum with superior antibacterial properties

Henry Agbe*, Dilip Kumar Sarkar, X.-Grant Chen,

Department of Applied Science, Aluminum Research Center – REGAL, University of Québec at Chicoutimi, Chicoutimi, QC, Canada, G7H 2B1.

*Corresponding author: henry.agbe@yahoo.co.uk

KEYWORDS: Silver phosphate nanoparticles; electrochemical synthesis; anodized aluminum; Ag_3PO_4 coated anodized aluminum; antibacterial coating.

Abstract

A two-step electrochemical deposition process has been deployed to fabricate Ag_3PO_4 antibacterial coating on anodized aluminum surface. Structural, morphological and chemical compositional analyses characterized by XRD, SEM and FTIR, confirm the formation of crystalline Ag_3PO_4 nanoparticles. The Ag_3PO_4 coated anodized aluminum resulted in 100% *Escherichia coli* (*E.coli*) bacteria inactivation. Furthermore, susceptibility and photocatalysis studies on powdered (5 μg/mL) Ag_3PO_4 nanoparticles showed excellent antibacterial properties with a zone of inhibition of 20 ± 1.3 mm and 100% *E.coli* inactivation under 15 min of visible-light irradiation. Additionally, the electrochemically synthesized Ag_3PO_4 coating on anodized aluminum exhibited a remarkably high adhesion.

1 Introduction

Silver is a metallic element of great value in human civilisation. It finds application in photography, catalysis and antimicrobial applications among many others [1]. In particular, antimicrobial property of silver has been known throughout history, and was used to fight microbial infections until the discovery of penicillin in the 1940s [2]. However, the inherent ability of microorganisms to mutate, coupled with indiscriminate use of antibiotics has resulted in the development of antimicrobial resistant strains to conventional antibiotics, necessitating the need for novel antimicrobial solutions. In this regard, nanotechnology can serve as an important toolkit for synthesizing variety of promising antimicrobial materials such as antimicrobial silver phosphate nanoparticles.

Silver phosphate (Ag_3PO_4) is a high quantum yield visible-light active photocatalytic nanomaterial [3]. Since its discovery by Yi et al.[4] in 2010, various groups have reported on the excellent photocatalytic performance of Ag_3PO_4 for various applications, including water purification, environmental remediation, water splitting and most importantly, the antibacterial applications [3, 5, 6]. Xie et al. [7] demonstrated an antibacterial property of silver phosphate using the synergistic effect of Ag^+ ion and reactive oxygen species (ROS) in both vitro and in vivo systems [7]. They showed that by immobilizing polydopamine (PDA)/Ag_3PO_4/graphene oxide (GO) coatings on both titanium alloy and polyether ether ketone (*PEEK*), the hybrid coating could maintain a repeatable and sustained antibacterial efficacy against both *Staphylococcus Aureus* (gram +ve) and *E.coli* (gram –ve). Similarly, in the work of Xu et al. [8], a synergistic antibacterial effects of nanospikes and Ag_3PO_4-TiO_2- photocatalyst was able to inactivate both *Staphylococcus Aureus* (gram +ve) and *E.coli* (gram –ve) bacteria under 20

min of visible light irradiation. Meanwhile, Zhang et al. [9] showed that nanocomposite power of polyvinyl alcohol hydrogel (PAH), reduced graphene oxide (RGO), molybdenum disulphide (MoS_2) and silver phosphate (Ag_3PO_4), under co-irradiation of 660 nm (visible light) and 808 nm (near-infrared light) could inactivate both *Staphylococcus aureus* and *E.coli* bacteria [9]. Note that antibacterial property of Ag_3PO_4, can also be enhanced by the PO_4^{3-}groups, which can attract bacteria in a "Trojan horse system", interfering with the Adenosine triphosphate/Adenosine diphosphate (ATP/ADP) interconversion cycle through competitive inhibition pathways to inactivate bacterial cell [10].

Conventionally, Ag_3PO_4 has been synthesized by ion exchange, precipitation and hydrothermal synthesis processes [11]. Hong et al., used hydrothermal method to fabricate a Bi_2S_3 nanorod (NR) arrays on titanium (Ti) implants, followed by a stepwise electrostatic adsorption of Ag_3PO_4 nanoparticles (NPs) [12]. While the coating demonstrated an excellent biocompatibility and antibacterial properties against both *Staphylococcus aureus* and *E.coli*, the adhesive property of the coating on the titanium implants was not reported. For application on frequently touched surfaces such as doorknobs and countertops, where coatings must adhere to underlying substrates, wet chemistry technique such as electrochemical deposition processes are desirable. Yi et al. [4] has reported Ag_3PO_4 synthesis by electrochemical process for deposition on indium tin-oxide (ITO)-coated glass substrate. However, their application was not focussed on antibacterial properties, but rather, on successful coating for water splitting application. Furthermore, electrochemical silver-phosphate synthesis has been limited to hydroxyapatite-based compounds [13-15] presumably due to their unique osseo-integration property as reported. Fu et al. [13] deplored a two-step electrochemical process to fabricate a

silver-hydroxyapatite (Ag-$Ca_{10}(PO_4)_6(OH)_2$) on titanium alloy surface for orthopaedics and dental implant applications. The titanium alloy was first coated with hydroxyapatite during the oxidation process, followed by silver nanoparticles deposition on the hydroxyapatite during the reduction process. Their silver-hydroxyapatite coated titanium alloy was effective in inhibiting the growth of gram (-) *E.coli* bacteria by 87% in a span of 8 h. In a similar study, Mokabber et al. [14] used a pulsed electrodeposition method to fabricate silver-calcium phosphate coatings on titanium substrates. The silver-calcium phosphate coatings exhibited an antibacterial efficiency between 76 to 99.7% for *Staphylococcus aureus* bacterium in 48 h. In a related study, Luo. et al. [16] fabricated a pyrrole/hydroxyapatite/ZnO-Ag-Cu nanocomposite coatings on Ti substrate using pulse electrochemical method. During the oxidation step, pyrrole was polymerized into polypyrrole, and then followed by nucleation and growth of hydroxyapatite (from PO_4^{3-}-based electrolyte) during the reduction step. This coating was not only effective in inactivating bacteria, but also in promoting growth and proliferation of both Vascular Endothelial Cells (VECs) and Bone Marrow Mesenchymal Stem Cells (BMSCs). From the foregoing, it is noticeable that reported work on electrochemical process has been limited to titanium alloys due to their biocompatibility [17-21]. However, as aluminum is a commonly used engineering material for general construction and fabrication of frequently touched surfaces, it is important the surface of such material be modified to exhibit antibacterial property via electrochemical process such as deposition of silver phosphate on the anodized aluminum oxide surfaces. Such surfaces could be installed in hospitals and public transport hubs to reduce microbial burden and healthcare associated infections.

In the present work, a two-step electrochemical process has been deployed to fabricate Ag_3PO_4 nanoparticles on anodized aluminum oxide for antibacterial applications. Ag^+ ion was first reduced to Ag^0 metal at a reduction process, while the metallic Ag^0 was oxidized again into Ag^+ ion. Antibacterial properties of the Ag_3PO_4 coated anodized aluminum (Ag_3PO_4/AAO/Al) were studied by a novel dry seeding, Kirby Bauer disk diffusion and photocatalytic assays, showing promising results for application on frequently touched aluminum parts.

2 Experimental section

2.1 Anodization of aluminum

AA6061-T6 aluminum sheet of dimensions 2.54 cm x 5.08 cm were degreased under ultrasound washing in a diluted soap solution (LIQUINOX), followed by distilled water washing for 15 minutes. Next, 1 M NaOH (VWR) chemical etching at 55 °C was performed for 3 minutes to remove the weak native oxide layer from the clean Al surfaces. The etched Al substrates were then immersed in HNO_3 solution (10 wt. %, VWR) for desmutting, followed by rinsing in distilled water. Subsequently, etched and desmutted Al alloys were anodized in an acidic electrolyte of 3 wt.% H_3PO_4 (VWR) in galvanostatic mode at a constant current density of 40 mA/cm^2 for 120 minutes. The electrochemical cell was equipped with a 600 W direct current power supply (Ametek Sorensen DCS 100-12E, Chicoutimi, QC, Canada), a quartz-jacketed beaker with circulating cold water (5 °C), and a small magnetic Teflon stirrer, rotating at 2000 rpm. Finally, the anodized aluminum oxide (AAO/Al) samples were dried at 70 ˚C overnight in an electric oven (VWR® Forced Air Ovens, Basic, 230V, Alberta, Canada). For quality control and reproducibility, each experiment was repeated in triplicate.

2.2 Electrochemical deposition of Ag_3PO_4 nanoparticles

A two-step redox electrochemical process was deployed to deposit Ag_3PO_4 nanoparticles in situ on anodized aluminum oxide layer (AAO/Al) in a regular two-electrode cell (Ametek Sorensen DCS 100-12E, Chicoutimi, QC, Canada),. In the first stage, AAO/Al and as-received aluminum (used as cathode and anode electrodes, respectively) were immersed in a 0.12 M $AgNO_3$ electrolyte solution under a -1.0 V DC potential and a temperature of 65 ± 1 °C, while stirring with a magnetic Teflon stirrer rotating at 500 rpm for 15, 30 and 60 minutes. In the second stage, electrodes were exchanged, where the Ag coated anodized aluminum oxide (Ag/AAO/Al) and as-received aluminum were used as anode and cathode, respectively. The electrodes were immersed in a 0.12 M sodium orthophosphate (Na_2HPO_4) electrolytic solution under a 10 V DC potential for 60 seconds at a temperature of 65 ± 1 °C. During this process, metallic Ag^0 oxidizes to react with orthophosphate anions (PO_4^{3-}) to form the Ag_3PO_4 [4] in situ on anodized aluminum pores. To investigate antibacterial activity in aqueous conditions, powder form of Ag_3PO_4 was also prepared by following a modified ion-exchange process described in our previous contribution [3]. Briefly, 0.12 M $AgNO_3$ was completely dissolved in 100 mL distilled water under constant magnetic stirring. Next 0.12 M of Na_2HPO_4 was added dropwise to the above solution under continuous stirring for 15 minutes to form the Ag_3PO_4 precipitate in the solution. The powdered Ag_3PO_4 was washed severally with deionised water, followed by drying at 70 ˚C overnight in an electric oven (VWR).

2.3 Sample characterization

The micro-nanostructure and morphological analyses were performed using Scanning Electron Microscopy (SEM, JEOL JSM-6480 LV, Pleasanton, USA). Elemental composition of the Ag_3PO_4 nanoparticles were further analyzed with the SEM equipped energy-dispersive spectroscopy (SEM, JEOL JSM-6480 LV, Pleasanton, USA). The crystalline structure and chemical composition were analyzed using X-ray powder diffraction (XRD) (a Bruker D8 Discover system, Ontario, Canada) and attenuated total reflection-Fourier transform infrared (ATR, Agilent Technologies Cary 630 FTIR, Santa Clara, USA), respectively. The XRD data are collected in the 2θ range of 10−80°, with a step size of 0.02°, while the FTIR spectra were collected in the range of 4000 – 500 cm^{-1}. Cross-Hatch Cutter, (ASTM D-3359, Rockville, USA) was used to evaluate adhesion level of the Ag_3PO_4 coated anodized aluminum.

2.4 Antibacterial assays. Antibacterial performances were determined by dry seeding, Kirby Bauer disk diffusion assays and photocatalysis**.** Dry seeding was performed as follows: The *E. coli* bacterium (ATCC 8739), was grown overnight from frozen (−80 °C) glycerol stock in tryptic soy broth (TSB) (Hardy Diagnostics, Santa Clara, USA) at 37 °C. A sub-culture was prepared on a fresh TSB (37 °C) to obtain bacterial cell density of 10^8 colony forming units/milliliter, (CFU)/mL. Cell density was determined at a wavelength of 625 nm at an absorbance of 0.1. Next, 5 µL of bacterial inoculum was seeded onto a sterile 2.54 cm x 2.54 cm Ag_3PO_4 coated anodized aluminum and control coupons. Coupons were incubated at ambient conditions of temperature (25 °C) and relative humidity (50 ± 10%) in a Class II Biological safety cabinet for a pre-determined contact time (0, 15, 60, 90, 240 and 1440 minutes). Sterile swab was then used to sample bacteria into a physiological saline (0.85 wt.%

NaCl), followed by serial dilutions and plating on tryptic soy agar (TSA). Agar plates were then aerobically incubated at a temperature of 37 °C for 24 h to yield countable viable bacterial colonies (30–300 colonies per plate). Three independent experiments were performed from fresh culture, and repeated to determine number of viable bacteria. Data were analyzed by a one-way analysis of variance (ANOVA) with the Tukey–Kramer multiple comparison test. Results were considered significant at $p < 0.05$. Antibacterial efficiency was calculated as: [(A-B)]/A×100 %, where A = colony-forming unit per cm^2 (CFU/cm^2) of viable bacteria on Ag_3PO_4 coated anodized aluminum coupon and B = CFU/cm^2 of viable bacteria on as-received aluminum coupon (as control).

The Kirby Bauer disk diffusion assay was prepared as described in our previous work [22]. Similar protocol described above was used to grow bacterial culture. For photocatalysis-mediated *E. coli* inactivation, 2g/L Ag_3PO_4 or commercially available TiO_2 anatase (positive control) powder were dispersed in physiological saline, containing *E.coli* inoculum. Next, the reactor flasks were exposed to either the visible light (25-watt table lamp, 17.3 W/m^2, Sigma-Aldrich Canada Co) or the UV-A light (30-watt UV-A lamp, 259 nm, 21 W/m^2, Sigma-Aldrich Canada Co) under constant stirring, with 1 ml aliquots withdrawn for pre-determined time of 0, 15, 30 and 60 minutes to determine bacteria concentration. This was determined by performing serial dilution, followed by streaking to obtain a bacterial lawn. After incubation at 37 ºC for 24 h, the number of viable *E. coli* cells were counted. Bacterial inactivation rate was calculated using the formula:

$$R\% = \left[\frac{C_0 - C_T}{C_0}\right] * 100\% \quad (1)$$

where, C_0 is the initial bacteria concentration, C_T is bacteria concentration at time T and R %, is the inactivation rate. All laboratory supplies, as well as coupons were sterilized at 121 °C for 30 minutes in autoclave prior to antibacterial study.

3 Results and Discussion

3.1 Deposition of Ag_3PO_4 on anodized aluminum oxide layer

A two-step redox electrochemical process was deployed to deposit Ag_3PO_4 in situ on an anodized aluminum oxide (AAO/Al) according to Equations 2 and 3.

Cathodic reaction:

$$Ag^{+} + e^{-} \rightarrow Ag_s \tag{2}$$

Anodic reaction:

$$3Ag_S^0 + PO_4^{3-} \rightarrow Ag_3PO_4 \downarrow + 3e^{-} \tag{3}$$

During the reduction process, a -1.0V potential reduces Ag^+ ion into metallic Ag^0 in situ on AAO/Al (Fig. 1(A)). Evidently, this is a typical current-time transient curve for instantaneous silver growth [23], where incoming silver atoms occupy all nucleation sites simultaneously at the instant of deposition [24]. As shown in Fig. 1(A), current density increased linearly with time and attained a maximum peak of 376 μA/cm^2 and 831 μA/cm^2 after 15 and 60 minutes of electrodeposition, respectively. It should be mentioned that the barrier oxide layer (~250 nm in thickness) of typical sulphuric acid anodized aluminum presents a challenge for metal electrodeposition [25]. Traditionally, two steps have been utilized for DC metal electrodeposition on anodized aluminum. These methods involve removal of base aluminum

metal with saturated $HgCl_2$ solution in the first step, and metallization of the anodized alumina, prior to electrodeposition using high applied voltage (> 5V) [25]. However, this is not only cumbersome and time consuming, but also the high applied potential leads to hydrogen gas evolution from water splitting, and an unstable coating [25].

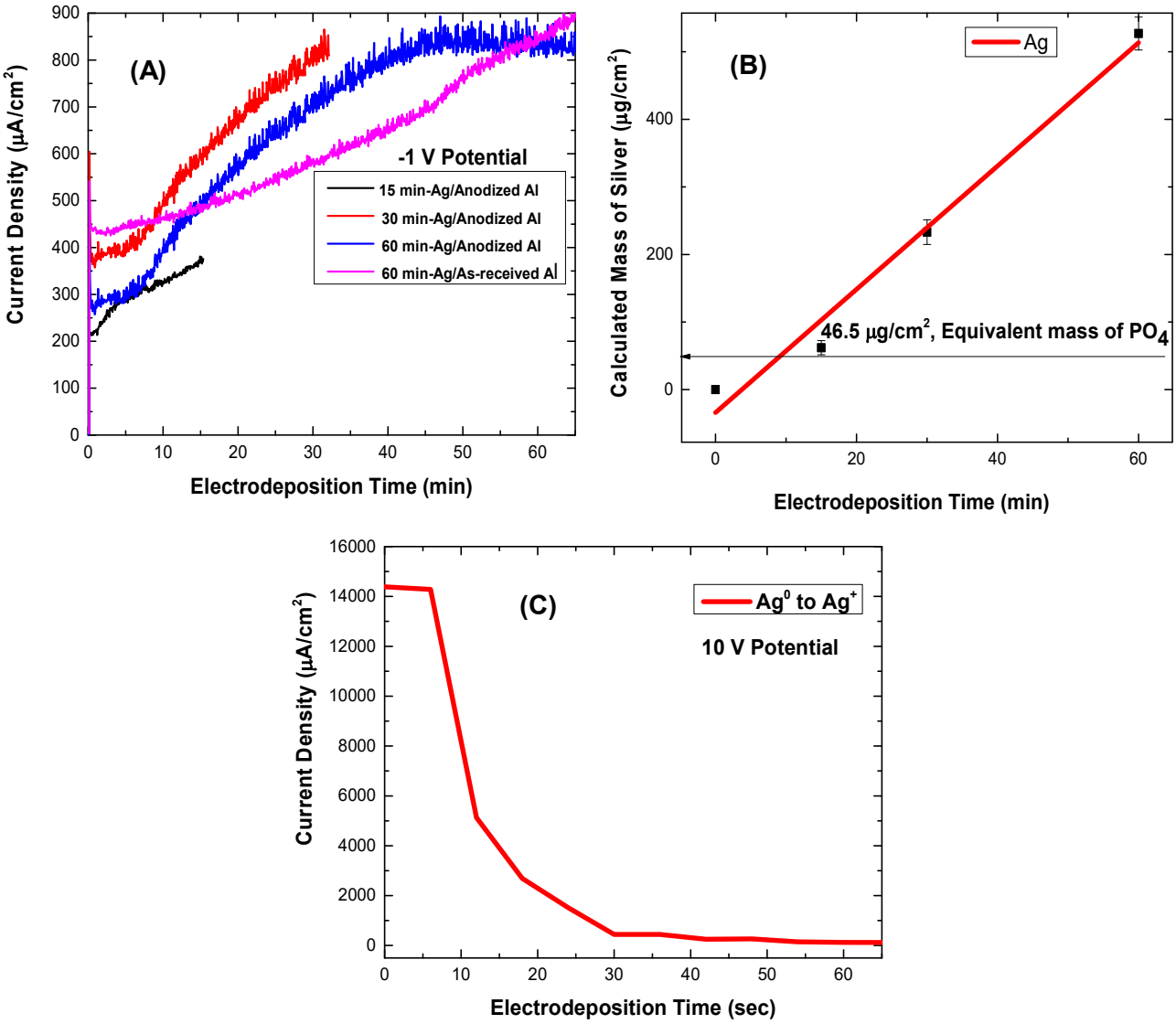

Fig. 1. Graphical representation of: (A) Current-time (I-t) transient curve of silver deposition on AAO/Al for 15, 30, and 60 minutes, (B) Calculated mass of Ag from (A); (C) Current-time (I-t) transient curve for electrodeposition of Ag_3PO_4 on AAO/Al

To circumvent this phenomenon, anodization of aluminum was performed with a 3 wt.% H_3PO_4 and the electrochemical silver reduction achieved at an optimal potential of -1.0V. The mass of silver determined from Equation 4, was found to increase linearly with deposition time (Fig. 1(B)), where, M is the molar mass of deposited Ag^0 (107.87 g mol^{-1}), or PO_4 (94.97 g mol^{-1}), *Z* is the number of electrons transferred or accepted in the redox reaction, *F* is Faraday's Constant (96,485 C/mol), I, the current (A) and t, the time (s)

$$m = \frac{\mathrm{MIt}}{ZF} \tag{4}$$

Calculated mass (mg/cm^2) of silver was 0, 0.062, 0.233 and 0.527 for electrodeposition time of 0, 15, 30 and 60 minutes, respectively and equivalent mass of PO_4 of 0.0465 mg/cm^2. (Supporting Information, Table S1). After deposition of Ag in AAO/Al, this electrode was used in the solution of Na_2HPO_4 to deposited Ag_3PO_4. Fig. 1(C) shows the current-time (I-t) transient curve on the growth of Ag_3PO_4 from the deposited Ag in the electrolyte of Na_2HPO_4, utilizing a constant voltage of +10 V. During the oxidation process, metallic Ag^0 oxidizes to Ag^+, which in turn reacts with Na_2HPO_4. Specifically, as metallic Ag^0 oxidizes, Ag^+ reacts with PO_4^{3-} to electrochemically precipitate Ag_3PO_4 [4] in situ on anodized aluminum (Ag_3PO_4/AAO/Al) according to Equation 5.

$$3AgNO_3 + Na_2HPO_4 \rightarrow Ag_3PO_4 \downarrow +2NaNO_3 + HNO_3 \tag{5}$$

It is observed that this reaction occurred faster and completed in just one minute of +10V. The applied potential, in particular, among other factors (concentration and pH of electrolyte) plays

an important role in electrodeposition. This is due to the fact that the number of active nucleation sites and growth of metallic silver are proportional to applied potential [24].

Morphological analysis of both anodized aluminum oxide (AAO/Al) and Ag_3PO_4 coated anodized aluminum (Ag_3PO_4/AAO/Al) were characterized by SEM. Fig. 2(A) shows the SEM micrograph of AAO/Al, exhibiting typical porous morphological features [22]. Fig. 2(B), (C) and (D) show SEM micrographs of Ag_3PO_4 deposited electrochemically on anodized aluminum using deposited silver for 15, 30 and 60 minutes, respectively. Evidently, the number density of Ag_3PO_4 nanoparticles increased linearly with electrodeposition time, where 15 minutes led to a randomly distributed and fewer particles of average size, 33 ± 9 nm (Fig. 2(B) and Supporting Information, Fig. S1). However, as the electrodeposition time increased to 30 minutes, the number density of the particles increased accordingly, as characterized by few isolated uncoated areas (Fig. 2(C)). With further increase in deposition time to 60 minutes, individual Ag_3PO_4 nanoparticles of size 91 ± 27 nm presumably merged together to form nanoclusters, covering the entire area, (Fig. 2(D) and Supporting Information, Fig. S1). Nanoclusters of Ag_3PO_4 appears to be deposited in situ on AAO/Al pores of diameter of 151 ± 37 nm, as shown in Figs. 2.(E) and (F).

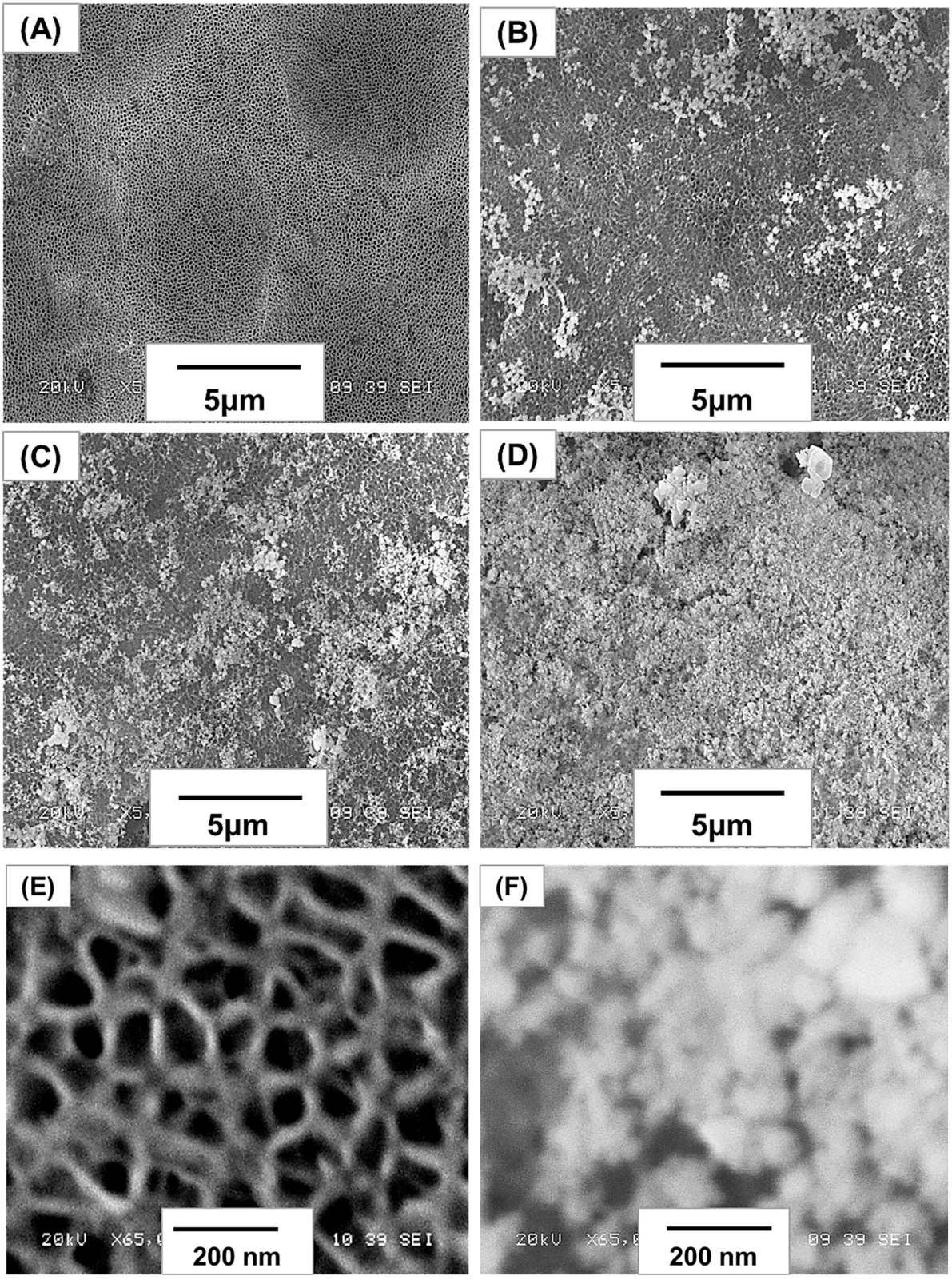
(A)
5µm
(B)
5µm
(C)
5µm
(D)
5µm
(E)
200 nm
(F)
200 nm

Fig. 1. SEM images of (A) AAO/Al; and electrodeposition of Ag_3PO_4 on AAO/Al using deposited silver for (B) 15 minutes; (C) 30 minutes; and (D) 60 minutes, respectively; and high magnification images of (E) AAO/Al and (F) Ag_3PO_4 on AAO/Al

Since chemical nature of Ag_3PO_4 coated anodized aluminum is important for determining Ag^+ release kinetics, a representative portion of Ag_3PO_4 coated anodized aluminum using 60 minutes deposited silver was examined using EDS elemental mapping. Among serval locations of the elemental mapping, Fig. 3(A) shows the SEM micrograph of the representative site, while the Figs. 3(B), (C), (D) and (E) show the elemental mapping of Al, O, Ag and P, respectively. Notably, Al and O, arising from porous oxide layer of AAO/Al covered the entire selected area (Fig. 3(B) and (C)), confirming the successful anodization. In addition, uniformly distributed patterns of Ag nanocluster are visibly distributed on entire selected area, as evident in Fig. 3(D). A similar trend was observed for P, albeit a low mass (Fig. 3(E)). It should be reiterated that a relative mass of 11.333 (Ag^+/PO_4) was observed for Ag_3PO_4 coated anodized aluminum. From both SEM micrograph and EDS elemental mapping, it is evident that Ag_3PO_4 nanoparticles was uniformly deposited on entire range of systematically selected area of the Ag_3PO_4 coated anodized aluminum. Additionally, EDS confirmed the elemental composition to consist of O, Al, and P (Fig. 3(F) and Fig. 4).

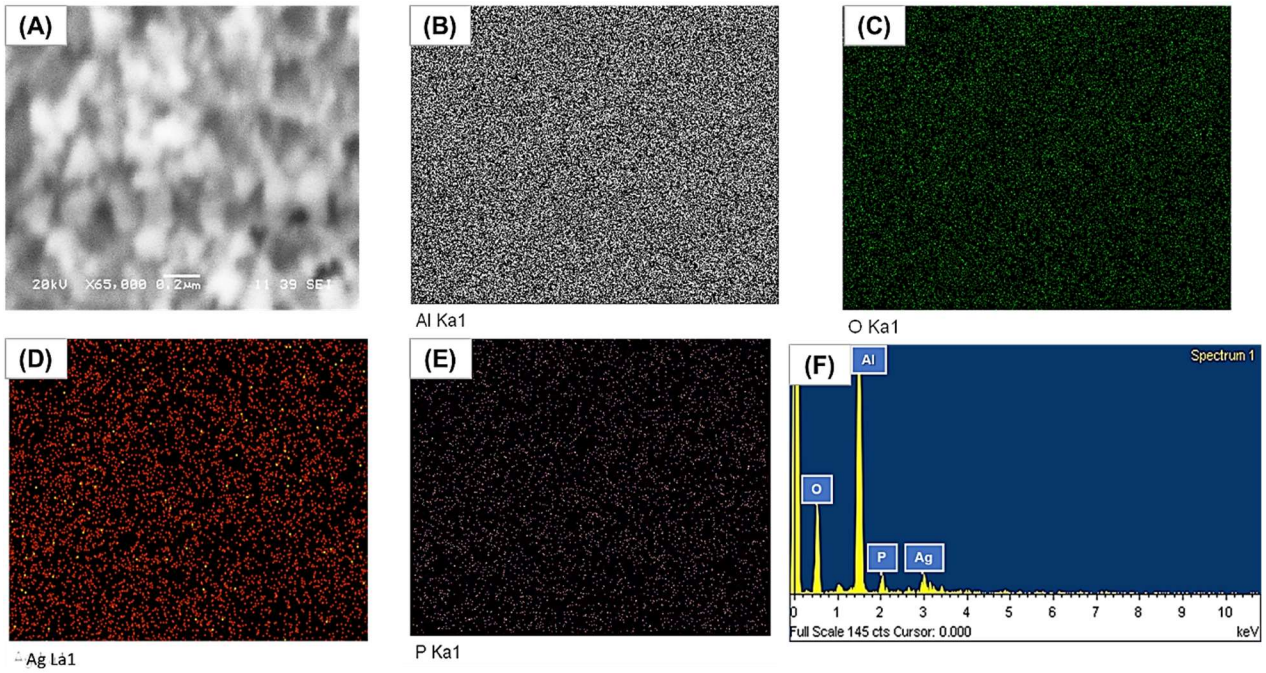

Fig. 2. EDS mapping of electrodeposition of Ag_3PO_4 on AAO/Al: (A) SEM image; (B) Al; (C) O; (D) Ag; (E) P; and (F) their elemental composition

As a further study, X-ray diffraction (XRD) analysis was performed to confirm the crystal structure of the Ag_3PO_4 coated anodized aluminum. Fig. 5(I-II)) shows the XRD spectra of body centered cubic (bcc) crystal structure of Ag_3PO_4 and the face centered cubic (fcc) structure of aluminum. All XRD patterns match well with standard data of Ag_3PO_4 with prominent peaks for 2θ at 20.8°, 29.7°, 33.3°, 36.5°, 42.4°, 47.8° 52.6°, 55.0°, 57.2°, 61.6°, 70.0°, 71.8° and 73.7°, with corresponding planes (110), (200), (210), (211), (220), (310), (222), (320), (321), (400), (411), (420) and (421), respectively (JCPDS No. 06-0505) [3]. The 2θ for aluminum of planes (200), (220) and (311), corresponds to 38.75°, 67.0° and 78.3, respectively (JCPDS file No. 04-

0787)[26]. These results show that the electrodeposited Ag_3PO_4 nanoparticles are of high crystallinity and purity.

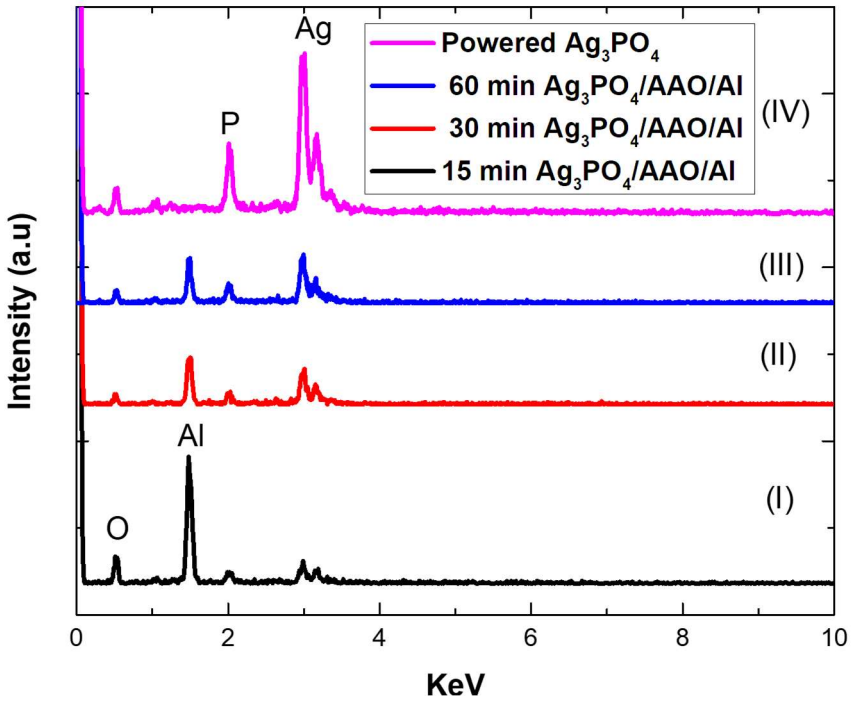

Fig. 3. EDS spectra of electrodeposition of Ag_3PO_4 on AAO/Al using deposited silver for (I) 15 minutes, (II) 30 minutes and (III) 60 minutes; and (IV) Powdered Ag_3PO_4, respectively.

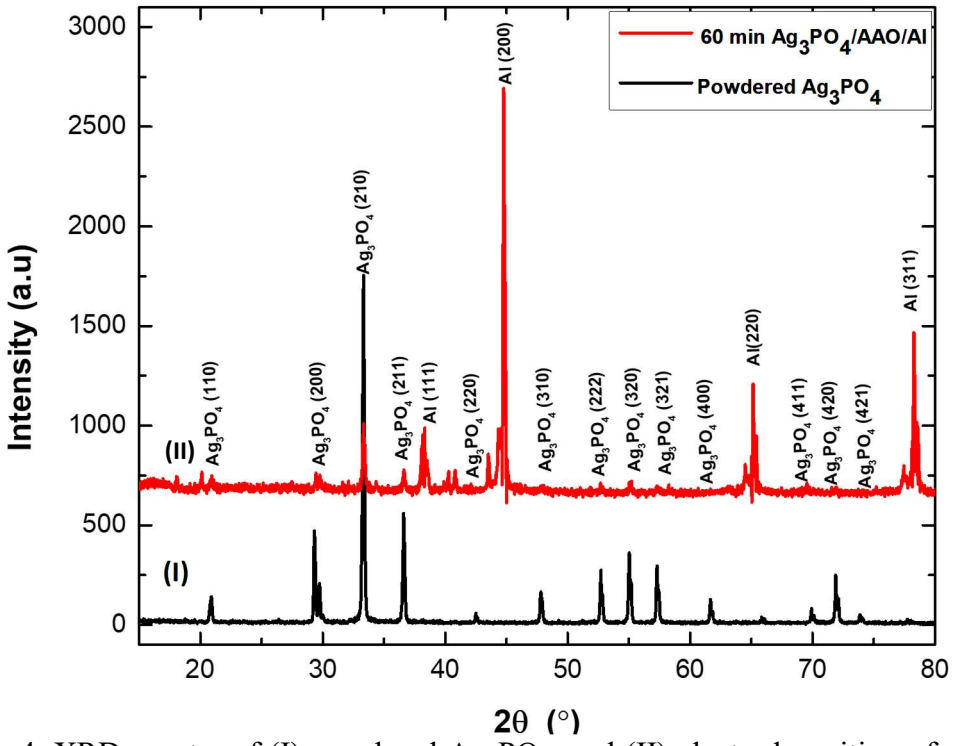

Fig. 4. XRD spectra of (I) powdered Ag_3PO_4; and (II) electrodeposition of Ag_3PO_4 on AAO/Al.

Fig. 6(A) shows the ATR-FTIR spectra of electrodeposition of Ag_3PO_4 on AAO/Al using deposited silver for 15, 30 and 60 minutes; and powdered Ag_3PO_4 (I-IV), respectively. The broad absorption bands of 3400–3500 cm^{-1} located at the high-frequency region can be assigned to the stretching vibration of H−O−H [27]. The two absorption peaks at the lower frequency region centered at 1650 cm^{-1}, correspond to bending vibration bond of O−H of absorbed water molecules, while the 1353 cm^{-1} can be attributed to the Ag−O vibration bond [28] of electrodeposited silver. Similarly, peaks at low frequency regions at 930 cm^{-1} and 550 cm^{-1} can be ascribed to the molecular vibrations of PO_4^{3-} and Ag – O bonds, respectively[28]. As expected, increased electrodeposition time, such as 60 minutes, increases intensity of Ag-O

absorption peaks at both 1353 cm^{-1} and 550 cm^{-1}. In addition, P-O peak appears to shift towards a lower frequency region as Ag-O peak increases. Contrarily to strong absorption peak associated with Ag-O vibration band at 1353 cm^{-1} for 60 minutes of electrodeposition, no signal was detected for the 15 and 30 minutes counterparts (Fig. 6(A) (I and 1I)). Furthermore, analysis of selected region of interest (560-540 cm^{-1}), confirmed a linear relation between the integrated peak area and electrodeposition time (Fig. 6(B). Thus, the coating obtained from 60 minutes of electrodeposition was selected for the remainder of the study.

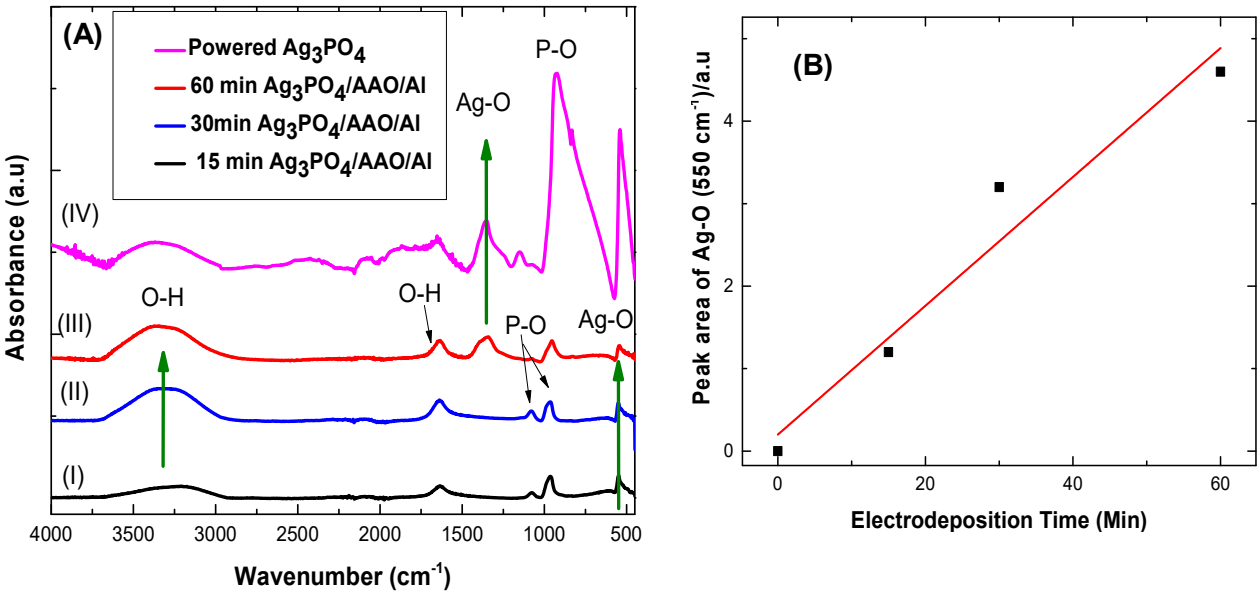

Fig. 5. (A) ATR-FTIR spectra of electrodeposition of Ag_3PO_4 on AAO/Al using deposited silver for (I) 15 minutes, (II) 30 minutes and (III) 60 minutes and (IV) Powdered Ag_3PO_4, respectively; and (B) Graphical representation of peak area with electrodeposition time.

Since the Ag_3PO_4 coated anodized aluminum is intended for frequently touched surfaces application, stability of such coatings is important. Therefore, a crosshatch adhesion tester based on ASTM D-3359 standard was used to evaluate the adhesion level of the Ag_3PO_4

coating with the anodized aluminum (Ag_3PO_4/AAO/Al). According to the ASTM standard, a grade 5B defines the highest level of adhesion of a coating with its substrate with the levels decreasing with lower grades, namely, 4B, 3B, 2B and 1B, while 0B defines the least adhesion level referring to very poor adhesion of the coating[29]. As evident from Fig. 7, electrodeposited Ag_3PO_4 on anodized aluminum (Ag_3PO_4/AAO/Al) exhibited the highest adhesion level of grade 5B, compared to electrodeposited Ag_3PO_4 on as-received aluminum with the lowest adhesion level of grade of 0B. The strong adhesion of Ag_3PO_4 coatings on anodized aluminum may be attributed to both anodization process and presence of P–O–P groups which interact covalently with Al_2O_3 to form P-O-Al via strong monodentate bonding [30]. Hence, Ag_3PO_4 coated anodized aluminum is found to be durable and therefore, ideal for practical applications.

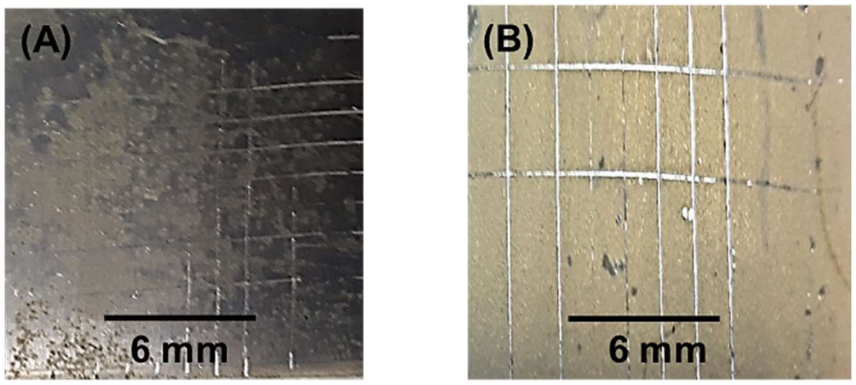

Fig. 6. Digital images of scratch test based on American Standard Test Method (ASTM D-3359) showing the adhesion of electrodeposited Ag_3PO_4 on (A) As-received aluminum and (B) AAO/Al.

3.2 Antibacterial assays

Antibacterial activity was studied by a novel dry seeding assay, Kirby Bauer disk diffusion assay and photo-induce catalysis. The dry seeding assay was performed to mimic near-dry conditions of frequently touched surfaces in hospital environments. The antibacterial performance of Ag_3PO_4/AAO/Al obtained from 60 minutes deposited silver was compared with control coupons such as copper, anodized aluminum oxide (AAO/Al) and as-received aluminum (Fig. 8).

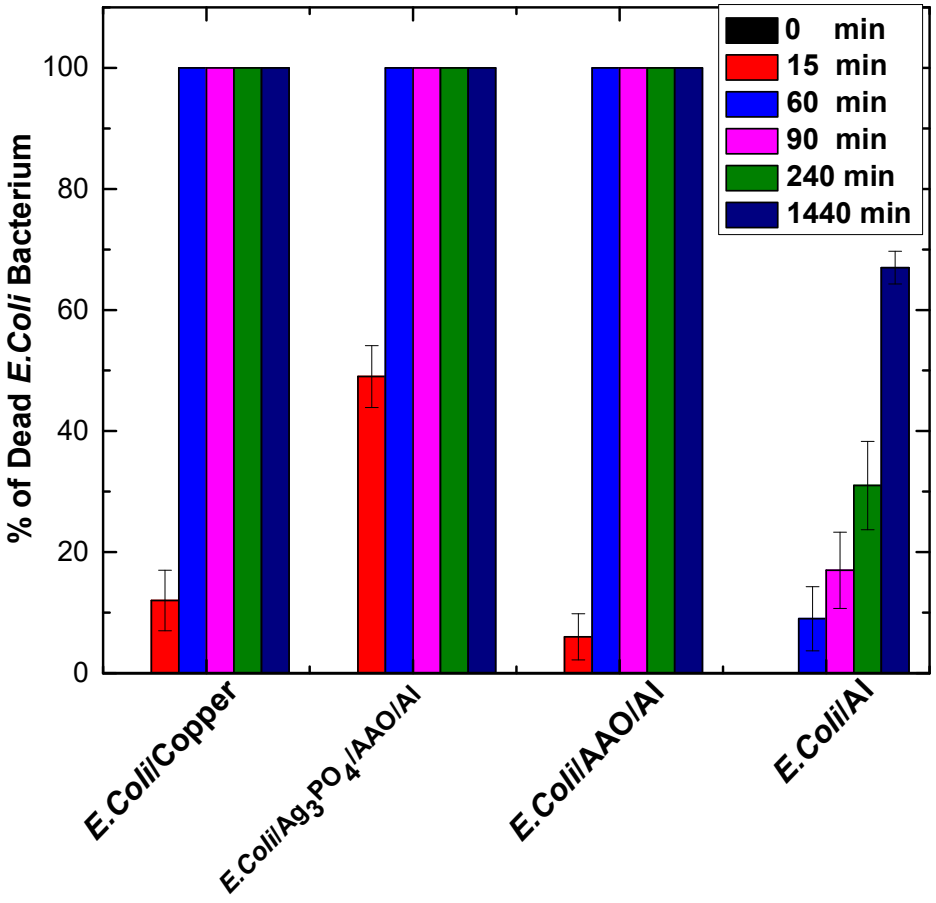

Fig. 7. Antibacterial activity of *E. coli* bacteria on Ag_3PO_4 coated anodized aluminum (Ag_3PO_4 /AAO/Al) compared to control samples (copper, AAO/Al and as-received aluminum) under different contact times.

Compared to copper and AAO/Al surfaces, which resulted in 12% and 6% *E.coli* bacteria death, respectively, Ag_3PO_4/AAO/Al, led to ~ 50% bacteria death in 15 minutes. However, after 60 minutes, a 100% bacteria killing was observed for all three conditions, which is consistent with other reports on copper [31, 32]. On the other hand, we found that AAO/Al is able to inactivate *E.coli* bacteria after 60 minutes of contact, which is presumably due to nanoscale topographical features of pore diameter, surface roughness, and oxide layer thickness. Anodizing aluminum with 3wt.% H_3PO_4 at a current density of 40 mA/cm^2 and anodization time of 120 minutes, exhibits a pore diameter of 151 ± 37 nm, a cell dimeter of 239 ± 53 nm, an oxide layer thickness of 5.3 ± 0.4 nm, a rms roughness of 2.9 ± 0.7μm and antibacterial efficiency of 100%. It should be mentioned that since topography-mediated antibacterial cicada wings was first reported by Ivanova and co-workers [33] against *Pseudomonas aeruginosa* (gram -ve) bacterium, and their subsequent report on synthetic analogue black silicon [34], these surfaces have attracted the interest of the scientific community due to their non-toxicity and durability. However, antibacterial mechanism of the topography-mediated antibacterial anodized aluminum is not provided here, this will be reported in our future contribution. Additionally, as can be seen, *E.coli* bacteria survived quite well on as-received aluminum. After 1440 minutes of bacterial contact, ~ 33% of *E.coli* bacteria was still persistent on as-received aluminum. This is worrisome; as such bacterial contaminated surface could lead to healthcare associated infections [35]. It has also been reported that multi-drug resistant (MDR) pathogens survive on inanimate dry high-touch surface for months [35-37]. Thus, our Ag_3PO_4/AAO/Al surfaces, which present better antibacterial effects, show sound promises to reduce both microbial burden and nosocomial infections in hygiene critical environment.

Antibacterial property of Ag_3PO_4 (5 µg/mL) was further analyzed using Kirby Bauer disk diffusion assay. Figs. 9(A) and (B) show the zone of inhibitions (ZOI) of *E.coli* bacteria by Ag_3PO_4 under visible light and dark conditions compared with commercially available antibacterial standard (as positive control) and deionized water (as negative control). The region surrounding an antibacterial agent where the growth of bacteria is inhibited or inactivated is called the zone of inhibitions (ZOI). The ZOI for Ag_3PO_4, under light and dark conditions were found to be 20 ± 1.3 mm and 15 ± 1.0 mm, respectively compared to 26 ± 1.7 mm for the commercially available standard. While the bacteria grew successfully around negative control sample. Antibacterial activity of Ag_3PO_4 in the dark conditions may be attributed to the presence of Ag^+. It should be mentioned that ~5 mm gain in ZOI by visible light activated Ag_3PO_4, is due to its photocatalytic nature.

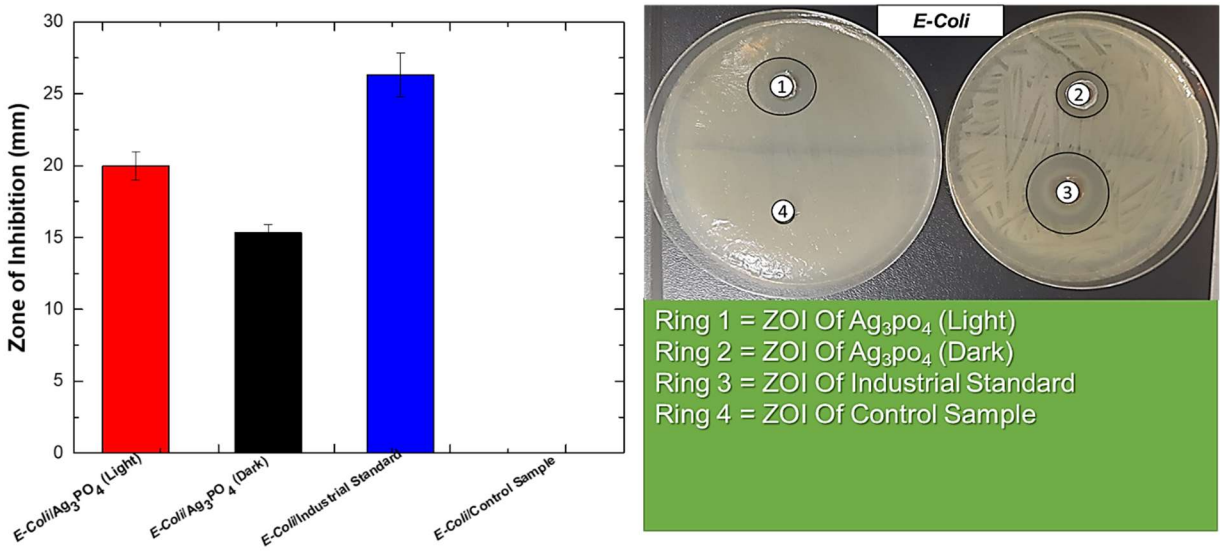

Fig. 8. (A). Antibacterial activity of powered Ag_3PO_4 nanoparticles against of *E. coli* (in both light and dark conditions) compared with controls (industrial standard and distilled water); and (B) Disk diffusion assay of Ag_3PO_4 nanoparticles: Ring 1 (Ag_3PO_4) (in light); Ring 2 (Ag_3PO_4) (in dark); Industrial

standard: Ring 3; Distilled water Ring 4. Data represent three independent experiments

These ZOI compare favourably with those reported on free releasing silver or silver-impregnated polymer. For example, ZOI of 19.5 ± 0.71 was observed for $AgNO_3$ (15 µg/mL) whilst a ZOI of 15.5 ± 0.71 has been reported for Derris trifoliate-Ag-NPs (10 µg/mL)[38].

Ag_3PO_4 is a photocatalyst [3], as such can be activated by visible light to generate Reactive Oxygen Species (ROS) to inhibit bacterial growth. Specifically, upon visible light activation by photons of energy greater than the bandgap of Ag_3PO_4 (2.34 eV > E_g of wavelength 530 nm), exciton or electron-hole pairs are generated [3], leading to ROS ($^{\bullet}OH^-$, $^{\bullet}O_2^-$ radicals, H_2O_2 etc.), which can inactivate bacterial cells [5]. Again, phosphate-uptake by bacteria can lead to Ag^+ ions release to covalently bond with both purine and pyrimidine base pairs, rupturing the H-bonds, leading to Deoxyribonucleic acid (DNA) disruption [39], loss of DNA replications [40] and bacterial death [41],[42]. Furthermore, Ag_3PO_4 is a slightly soluble in water (0.02 g/L 25 °C) and can release Ag^+ ions by sustained kinetic profile with oligodynamic effects [10]. Specifically, Ag_3PO_4 can dissociate gradually from $Ag_2PO_4^{1-}$ through $AgPO_4^{2-}$, to PO_4^{3-}. The PO_4^{3-}ions could then act as bait (in a "Trojan horse system") for targeting and interfering with ATP/ADP interconversion cycle to inactivate E. coli cell [10], (Fig. 10).

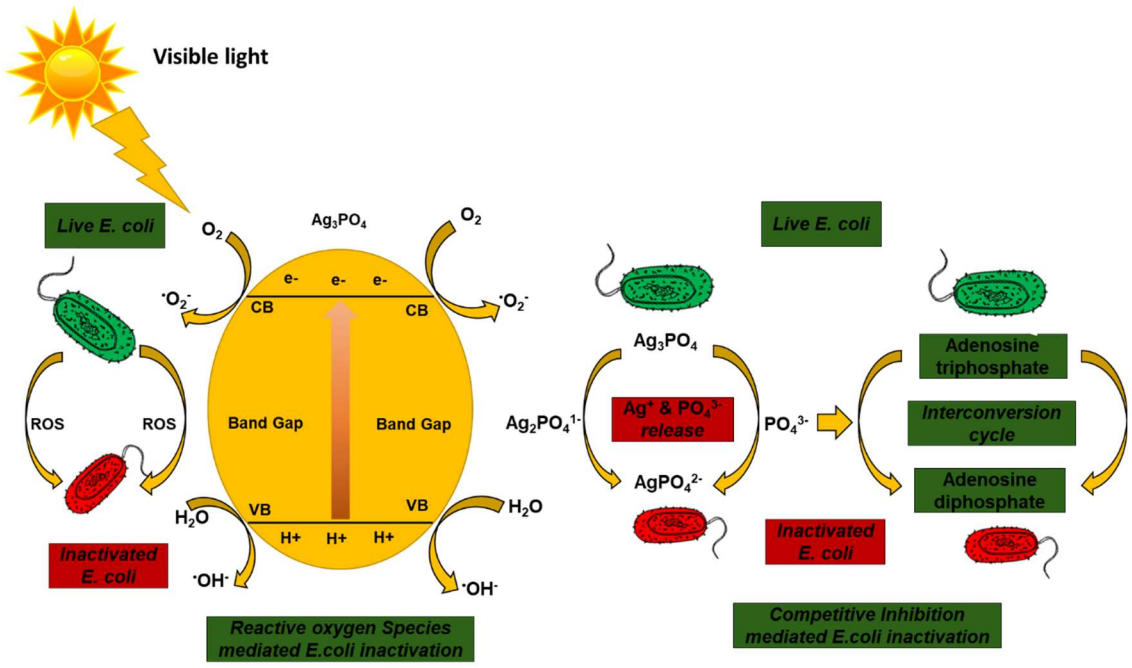

Fig. 10. Schematic representation of proposed mechanisms of antibacterial Ag_3PO_4 nanoparticles. Irradiating Ag_3PO_4 with visible light generates electron-hole pairs. Electrons at the conduction band edge (CB) reduces molecular oxygen into superoxide radicals ($\cdot O2^-$). Contrarily, hole on valence band edge (VB) oxidizes water into a highly hydroxyl radicals ($\cdot OH^-$). The generated reactive oxygen species (ROS) can participate to inactive E.coli cell. In addition, PO_4^{3-}ions could interfere with the Adenosine triphosphate/Adenosine diphosphate (ATP/ADP) interconversion cycle through competitive inhibition pathways to inactivate E.coli cell.

Per the Clinical and Laboratory Standards Institute standards, ZOI values falling within 8–30 mm are considered as acceptable standards for inactivating MDR pathogens such as

methicillin-resistant *Staphylococcus aureus* (MRSA), *Pseudomonas aeruginosa* and *E.coli* [43]. Therefore, Ag_3PO_4 proves to be an effective antibacterial agent, particularly for gram-negative bacteria, such as *E-coli.*

As factors such as humidity, temperature, concentration and light source affect antibacterial property of Ag_3PO_4, further analysis was performed for Ag_3PO_4 in aqueous conditions under both ultraviolet (UV) and visible-light irradiation. Fig. 11 shows *E.coli* inactivation rate under visible light, UV and dark conditions. As it is evident in Fig. 11 (A), Ag_3PO_4 under visible light proves to be very effective at inactivating *E.coli* bacteria. It achieved a 100% efficiency in 15 minutes compared to 44% by TiO_2 (titania), that was used as control (Supporting Information can be found in Table S2). Note that the titania is regarded as standard photocatalyst against which other photo catalytic materials are evaluated [44]. After 60 minutes of the photocatalysis, only 48% of *E.coli* bacteria had been inactivated by titania. Similarly, under 60 minutes visible light irradiation (without a Titania and Ag_3PO_4), only 13% of *E.coli* bacteria was inactivated. This signifies the role of catalysts (Ag_3PO_4 and TiO_2) in photocatalysis. Fig. 11 (B), shows the effect of photocatalysis under UV light. Similar to visible light, irradiation of Ag_3PO_4 by UV light led to 100% inactivation efficiency in 15 minutes. On the other hand, titania under same conditions, led to 70% inactivation efficiency. Increasing duration of irradiation of titania by UV light to 60 minutes, resulted in corresponding increase in *E. coli* bacteria inactivation efficiency by ~85% . This is ~100% increase in inactivation rate compared to titania under visible light conditions, which exhibited in an inactivation efficiency of 48% (Fig. 11 (A)). The high antibacterial performance of TiO_2 in the UV spectrum is presumably due to its high band gap range of 3.0–3.2 eV [45].

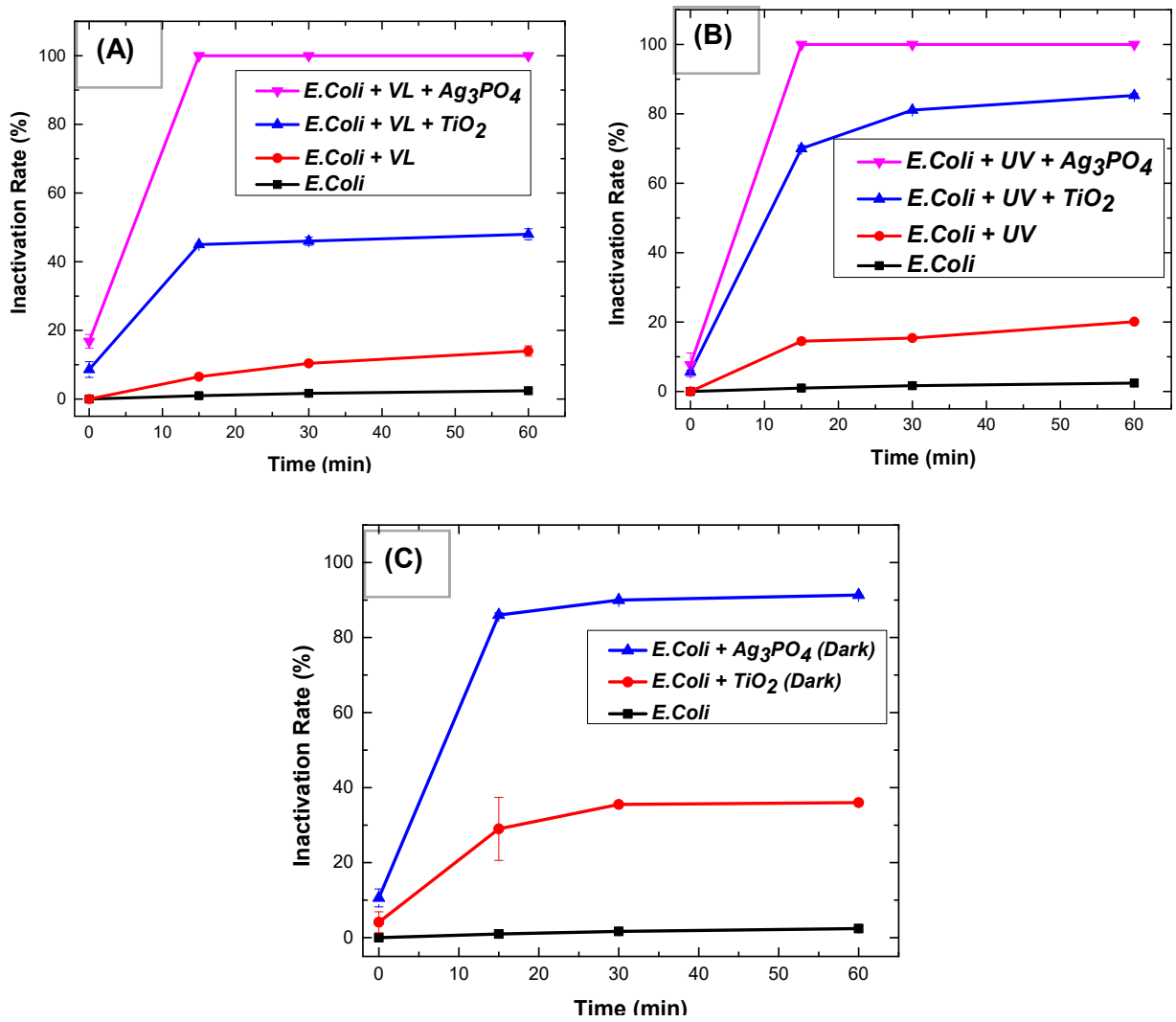

Fig. 11. *E. coli* bacterium inactivation by powdered Ag_3PO_4 nanoparticles under (A) Visible light irradiation; (B) UV-A irradiation; and (C) Dark condition. Data represent three independent experiments.

Thus, TiO_2 activation under UV light is much favourable than visible light. On the contrary, Ag_3PO_4 is photoactive in both UV and visible light spectra due to its low indirect and direct

band gaps of 2.36 and 2.43 eV [3], hence resulting in 100% efficiency as compared to TiO_2. As expected, efficiencies in dark were rather low, particularly for TiO_2, which exhibited ~ 36% efficiency after 60 minutes whereas that for Ag_3PO_4 was 91% (Fig. 11 (C)). The high *E.coli* inactivation rate for Ag_3PO_4 under same conditions can be attributed to the role of Ag^+ ions as explained above. While many reports exist in the literature relating to Ag_3PO_4 photocatalysis for water spitting and environmental degradation [4, 46-48] few reports are found on antibacterial application [49, 50] (Supporting information can be found in table S3). In the work of Seo et al.[49] for example, Ag_3PO_4 synthesized by precipitation method, yielded ~ 50% *E.coli* bacteria inactivation after 16 h, compared to 100% inactivation under only 15 minutes in our present study. In another work by Su et al.[50], a 99.91% *E.coli* bacteria inactivation was achieved by solvothermal synthesis of Ag_3PO_4/α-Fe_2O_3 composites. However, given the different experimental conditions reported in the literature direct comparisons must be treated with caution.

4 Conclusion

In the present study, Ag_3PO_4 was synthesized on anodized aluminum oxide (AAO/Al) by a two-step electrochemical process. Ag^+ ion was reduced to metallic Ag^0, followed by oxidation in sodium orthophosphate to form Ag_3PO_4 on AAO/Al. The Ag_3PO_4 coated anodized aluminum (Ag_3PO_4/AAO/Al) exhibited an excellent antibacterial efficiency of 100% for *E.coli* bacteria in 60 minutes. Both susceptibility and photocatalysis studies on Ag_3PO_4 showed excellent antibacterial properties, with ZOI value of 20 ± 1.3 mm and 100% *E.coli* inactivation under 15 minutes visible-light irradiation, respectively. Furthermore, the Ag_3PO_4 coated anodized aluminum exhibited a remarkably high adhesion levels of Ag_3PO_4 with the anodized

aluminum surfaces. Overall, the Ag_3PO_4 coated anodized aluminum has proven to be an excellent antibacterial material and a promising solution to be considered for use of frequently touched parts as adjunct to hand hygiene in reducing the potential threat of healthcare associated infections in hygiene critical environment**.**

Acknowledgements

We acknowledge the financial support from Fonds de recherche du Québec - Nature et technologies (FRQNT) under the grant number 2018-LU-210883. Authors thank Dr. Saleema Noormohammed for the critical reading and improving the quality of the manuscript.

References:

[1] A.B. Lansdown, Silver in healthcare: its antimicrobial efficacy and safety in use, Royal Society of Chemistry, 2010.
[2] A.J. Huh, Y.J. Kwon, "Nanoantibiotics": a new paradigm for treating infectious diseases using nanomaterials in the antibiotics resistant era, Journal of controlled release, 156 (2011) 128-145.
[3] H. Agbe, N. Raza, D. Dodoo-Arhin, A. Chauhan, R.V. Kumar, H2O2 rejuvenation-mediated synthesis of stable mixed-morphology Ag3PO4 photocatalysts, Heliyon, 4 (2018) e00599.
[4] Z. Yi, J. Ye, N. Kikugawa, T. Kako, S. Ouyang, H. Stuart-Williams, H. Yang, J. Cao, W. Luo, Z. Li, An orthophosphate semiconductor with photooxidation properties under visible-light irradiation, Nature materials, 9 (2010) 559-564.
[5] G. Panthi, R. Ranjit, H.-Y. Kim, D.D. Mulmi, Size dependent optical and antibacterial properties of Ag3PO4 synthesized by facile precipitation and colloidal approach in aqueous solution, Optik, 156 (2018) 60-68.
[6] A. Wu, C. Tian, W. Chang, Y. Hong, Q. Zhang, Y. Qu, H. Fu, Morphology-controlled synthesis of Ag3PO4 nano/microcrystals and their antibacterial properties, Materials Research Bulletin, 48 (2013) 3043-3048.
[7] X. Xie, C. Mao, X. Liu, L. Tan, Z. Cui, X. Yang, S. Zhu, Z. Li, X. Yuan, Y. Zheng, Tuning the bandgap of photo-sensitive polydopamine/Ag3PO4/graphene oxide coating for rapid, noninvasive disinfection of implants, ACS central science, 4 (2018) 724-738.
[8] Y. Xu, X. Liu, Y. Zheng, C. Li, K.W.K. Yeung, Z. Cui, Y. Liang, Z. Li, S. Zhu, S. Wu, Ag3PO4 decorated black urchin-like defective TiO2 for rapid and long-term bacteria-killing under visible light, Bioactive materials, 6 (2021) 1575-1587.

[9] C. Zhang, J. Wang, R. Chi, J. Shi, Y. Yang, X. Zhang, Reduced graphene oxide loaded with MoS2 and Ag3PO4 nanoparticles/PVA interpenetrating hydrogels for improved mechanical and antibacterial properties, Materials & Design, 183 (2019) 108166.
[10] J.-K. Liu, C.-X. Luo, J.-D. Wang, X.-H. Yang, X.-H. Zhong, Controlled synthesis of silver phosphate crystals with high photocatalytic activity and bacteriostatic activity, CrystEngComm, 14 (2012) 8714-8721.
[11] X. Li, P. Xu, M. Chen, G. Zeng, D. Wang, F. Chen, W. Tang, C. Chen, C. Zhang, X. Tan, Application of silver phosphate-based photocatalysts: Barriers and solutions, Chemical Engineering Journal, 366 (2019) 339-357.
[12] L. Hong, X. Liu, L. Tan, Z. Cui, X. Yang, Y. Liang, Z. Li, S. Zhu, Y. Zheng, K.W.K. Yeung, Rapid Biofilm Elimination on Bone Implants Using Near-Infrared-Activated Inorganic Semiconductor Heterostructures, Advanced healthcare materials, 8 (2019) 1900835.
[13] C. Fu, X. Zhang, K. Savino, P. Gabrys, Y. Gao, W. Chaimayo, B.L. Miller, M.Z. Yates, Antimicrobial silver-hydroxyapatite composite coatings through two-stage electrochemical synthesis, Surface and Coatings Technology, 301 (2016) 13-19.
[14] T. Mokabber, H. Cao, N. Norouzi, P. van Rijn, Y. Pei, Antimicrobial electrodeposited silver-containing calcium phosphate coatings, ACS applied materials & interfaces, 12 (2020) 5531-5541.
[15] S. Eraković, A. Janković, D. Veljović, E. Palcevskis, M. Mitrić, T. Stevanović, D. Janaćković, V. Mišković-Stanković, Corrosion stability and bioactivity in simulated body fluid of silver/hydroxyapatite and silver/hydroxyapatite/lignin coatings on titanium obtained by electrophoretic deposition, The Journal of physical chemistry B, 117 (2013) 1633-1643.
[16] J. Luo, B. Mamat, Z. Yue, N. Zhang, X. Xu, Y. Li, Z. Su, C. Ma, F. Zang, Y. Wang, Multi-metal ions doped hydroxyapatite coatings via electrochemical methods for antibacterial and osteogenesis, Colloid and Interface Science Communications, 43 (2021) 100435.
[17] S. Minagar, C.C. Berndt, J. Wang, E. Ivanova, C. Wen, A review of the application of anodization for the fabrication of nanotubes on metal implant surfaces, Acta biomaterialia, 8 (2012) 2875-2888.
[18] L. Visai, L. De Nardo, C. Punta, L. Melone, A. Cigada, M. Imbriani, C.R. Arciola, Titanium oxide antibacterial surfaces in biomedical devices, The International journal of artificial organs, 34 (2011) 929-946.
[19] D. Regonini, A. Satka, A. Jaroenworaluck, D.W. Allsopp, C.R. Bowen, R. Stevens, Factors influencing surface morphology of anodized TiO2 nanotubes, Electrochimica Acta, 74 (2012) 244-253.
[20] U.F. Gunputh, H. Le, R.D. Handy, C. Tredwin, Anodised TiO 2 nanotubes as a scaffold for antibacterial silver nanoparticles on titanium implant, Materials Science and Engineering: C, (2018).
[21] N. Somsanith, Y.-K. Kim, Y.-S. Jang, Y.-H. Lee, H.-K. Yi, J.-H. Jang, K.-A. Kim, T.-S. Bae, M.-H. Lee, Enhancing of Osseointegration with Propolis-Loaded TiO2 Nanotubes in Rat Mandible for Dental Implants, Materials, 11 (2018) 61.
[22] H. Agbe, D.K. Sarkar, X.-G. Chen, N. Faucheux, G. Soucy, J.-L. Bernier, Silver–Polymethylhydrosiloxane Nanocomposite Coating on Anodized Aluminum with Superhydrophobic and Antibacterial Properties, ACS Applied Bio Materials, 3 (2020) 4062-4073.
[23] S.C. Lai, R.A. Lazenby, P.M. Kirkman, P.R. Unwin, Nucleation, aggregative growth and detachment of metal nanoparticles during electrodeposition at electrode surfaces, Chemical science, 6 (2015) 1126-1138.
[24] D. Sarkar, X. Zhou, A. Tannous, K. Leung, Growth mechanisms of copper nanocrystals on thin polypyrrole films by electrochemistry, The Journal of Physical Chemistry B, 107 (2003) 2879-2881.
[25] F. Nasirpouri, Electrodeposition of nanostructured materials, Springer, 2017.
[26] R. Narayanasamy, T. Ramesh, M. Prabhakar, Effect of particle size of SiC in aluminium matrix on workability and strain hardening behaviour of P/M composite, Materials Science and Engineering: A, 504 (2009) 13-23.

[27] G. Huang, Y. Zhu, Enhanced photocatalytic activity of ZnWO4 catalyst via fluorine doping, The Journal of Physical Chemistry C, 111 (2007) 11952-11958.
[28] C. Piccirillo, R. Pinto, D. Tobaldi, R. Pullar, J. Labrincha, M. Pintado, P.M. Castro, Light induced antibacterial activity and photocatalytic properties of Ag/Ag3PO4-based material of marine origin, Journal of Photochemistry and Photobiology A: Chemistry, 296 (2015) 40-47.
[29] A. Milionis, E. Loth, I.S. Bayer, Recent advances in the mechanical durability of superhydrophobic materials, Advances in colloid and interface science, 229 (2016) 57-79.
[30] X. Chen, Y. Zheng, Y. Chen, Y. Xu, F. Zhong, W. Zhang, Y. Xiao, Y. Zheng, Improved methane oxidation activity of P-doped γ-Al2O3 supported palladium catalysts by tailoring the oxygen mobility and electronic properties, International Journal of Hydrogen Energy, 44 (2019) 27772-27783.
[31] J. Noyce, H. Michels, C. Keevil, Use of copper cast alloys to control Escherichia coli O157 cross-contamination during food processing, Applied and environmental microbiology, 72 (2006) 4239-4244.
[32] G. Grass, C. Rensing, M. Solioz, Metallic copper as an antimicrobial surface, Applied and environmental microbiology, 77 (2011) 1541-1547.
[33] J. Hasan, H.K. Webb, V.K. Truong, S. Pogodin, V.A. Baulin, G.S. Watson, J.A. Watson, R.J. Crawford, E.P. Ivanova, Selective bactericidal activity of nanopatterned superhydrophobic cicada Psaltoda claripennis wing surfaces, Applied microbiology and biotechnology, 97 (2013) 9257-9262.
[34] E.P. Ivanova, J. Hasan, H.K. Webb, G. Gervinskas, S. Juodkazis, V.K. Truong, A.H. Wu, R.N. Lamb, V.A. Baulin, G.S. Watson, Bactericidal activity of black silicon, Nature communications, 4 (2013) 1-7.
[35] A. Kramer, I. Schwebke, G. Kampf, How long do nosocomial pathogens persist on inanimate surfaces? A systematic review, BMC infectious diseases, 6 (2006) 130.
[36] R.A. Weinstein, B. Hota, Contamination, disinfection, and cross-colonization: are hospital surfaces reservoirs for nosocomial infection?, Clinical infectious diseases, 39 (2004) 1182-1189.
[37] V. Russotto, A. Cortegiani, T. Fasciana, P. Iozzo, S.M. Raineri, C. Gregoretti, A. Giammanco, A. Giarratano, What healthcare workers should know about environmental bacterial contamination in the intensive care unit, BioMed research international, 2017 (2017).
[38] N. Cyril, J.B. George, L. Joseph, A. Raghavamenon, S. VP, Assessment of antioxidant, antibacterial and anti-proliferative (lung cancer cell line A549) activities of green synthesized silver nanoparticles from Derris trifoliata, Toxicology research, 8 (2019) 297-308.
[39] S.L. Banerjee, P. Potluri, N.K. Singha, Antimicrobial cotton fibre coated with UV cured colloidal natural rubber latex: A sustainable material, Colloids and Surfaces A: Physicochemical and Engineering Aspects, 566 (2019) 176-187.
[40] K. Zheng, M.I. Setyawati, D.T. Leong, J. Xie, Antimicrobial silver nanomaterials, Coordination Chemistry Reviews, 357 (2018) 1-17.
[41] S.L. Percival, A.-M. Salisbury, R. Chen, Silver, biofilms and wounds: resistance revisited, Critical reviews in microbiology, (2019) 1-15.
[42] L.C. Gerber, D. Mohn, G. Fortunato, M. Astasov-Frauenhoffer, T. Imfeld, T. Waltimo, M. Zehnder, W.J. Stark, Incorporation of reactive silver-tricalcium phosphate nanoparticles into polyamide 6 allows preparation of self-disinfecting fibers, Polymer Engineering & Science, 51 (2011) 71-77.
[43] P. Wayne, Clinical and laboratory standards institute. Performance standards for antimicrobial susceptibility testing, (2011).
[44] H. Agbe, E. Nyankson, N. Raza, D. Dodoo-Arhin, A. Chauhan, G. Osei, V. Kumar, K.-H. Kim, Recent advances in photoinduced catalysis for water splitting and environmental applications, Journal of Industrial and Engineering Chemistry, 72 (2019) 31-49.
[45] R. Abe, K. Hara, K. Sayama, K. Domen, H. Arakawa, Steady hydrogen evolution from water on Eosin Y-fixed TiO2 photocatalyst using a silane-coupling reagent under visible light irradiation, Journal of Photochemistry and Photobiology A: Chemistry, 137 (2000) 63-69.

[46] N. Raeisi-Kheirabadi, A. Nezamzadeh-Ejhieh, A Z-scheme g-C3N4/Ag3PO4 nanocomposite: Its photocatalytic activity and capability for water splitting, International Journal of Hydrogen Energy, 45 (2020) 33381-33395.
[47] H. Yin, Y. Cao, T. Fan, M. Zhang, J. Yao, P. Li, S. Chen, X. Liu, In situ synthesis of Ag3PO4/C3N5 Z-scheme heterojunctions with enhanced visible-light-responsive photocatalytic performance for antibiotics removal, Science of The Total Environment, 754 (2021) 141926.
[48] O. Altan, Ö. Metin, Boosting formic acid dehydrogenation via the design of a Z-scheme heterojunction photocatalyst: The case of graphitic carbon nitride/Ag/Ag3PO4-AgPd quaternary nanocomposites, Applied Surface Science, 535 (2021) 147740.
[49] Y. Seo, B.-E. Yeo, Y.-S. Cho, H. Park, C. Kwon, Y.-D. Huh, Photo-enhanced antibacterial activity of Ag3PO4, Materials Letters, 197 (2017) 146-149.
[50] W. Su, X. Liu, L. Tan, Z. Cui, Y. Liang, Z. Li, S. Zhu, S. Wu, Rapid Sterilization by Photocatalytic Ag3PO4/α-Fe2O3 Composites Using Visible Light, ACS Sustainable Chemistry & Engineering, 8 (2020) 2577-2585.